J Nanostruct 15(1): 65-74, Winter 2025

RESEARCH PAPER

Morphological and Structural Analysis of ZnO-Doped TiO_2 Nanostructures Via Low-Temperature CBD for Sensing Application

Hayder Mousa Neamah [1], Hayder Mohsin Jasim [2], Mohsin Hamzah Abed [3]*

[1] *College of Education, Department of Physics, University of Al-Qadisiyah, Iraq*
[2] *College of Basic Education, Al-Mustansiriya University, Iraq*
[3] *Ministry of Education, Iraq*

ARTICLE INFO

Article History:
Received 11 August 2024
Accepted 23 December 2024
Published 01 January 2025

Keywords:
ZnO-TiO_2 Nanostructures
Chemical Bath Deposition (CBD)
NH_3 Gas Sensor

ABSTRACT

In this study, ZnO-TiO_2 nanostructures were successfully synthesized via a low-temperature chemical bath deposition (CBD) method for NH_3 gas sensing applications. TiO_2 doping concentrations (5% and 20%) were investigated to optimize the sensing performance. Structural analysis verified hexagonal wurtzite ZnO and anatase TiO_2 formation. FE-SEM showed semi-spherical particles averaging 17.96 nm for ZnO and 39.1 nm for TiO_2. The gas sensing results demonstrated superior performance for the 20% TiO_2-doped sample, exhibiting a sensitivity of 135% at 100 ppm NH_3, compared to 110% for the 5% sample. Furthermore, the 20% TiO2-doped sensor showed enhanced response kinetics with a faster response time of 35 seconds and recovery time of 95 seconds, compared to 45 seconds and 120 seconds respectively, for the 5% sample. This improved performance is attributed to the formation of optimal n-n heterojunctions at the ZnO-TiO_2 interface, increased oxygen vacancies, and enhanced electron transport network, making the 20% TiO_2-doped ZnO nanostructure an efficient room-temperature NH_3 gas sensing material.

How to cite this article
Neamah H., .Jasim H., Abed M. Morphological and Structural Analysis of ZnO-Doped TiO_2 Nanostructures Via Low-Temperature CBD for Sensing Application. J Nanostruct, 2025; 15(1):65-74. DOI: 10.22052/JNS.2025.01.007

INTRODUCTION

Making solar cells have high absorption factor necessitates utilization of antireflection coatings. Currently, a number of NaStructured materials is being investigated for ability to control light and improve light trapping aSWell as light absorption effect in photovoltaic (PV) cells. It is widely known that zinc oxide possesses tunable optical and electrical properties, which makes it possible to consider it for optoelectronic uses [1]. The quantitative analysis of the recent investigations revealing the density of the defect centers in the ZnO lattice influences the optical, magnetic, and electrical properties of ZnO nanostructures.[2]. Out of the transition metals, the result shows that titanium is an ideal dopant for ZnO because it has similar ionic radii, richer electronic energy levels and actually a divalent transition metal[3]. Furthermore, with a low titanium concentration in ZnO (below 2.0 at.%), titanium-doped ZnO exhibits comparatively strong optical and magnetic characteristics [4]. Numerous techniques, including sputtering, sol gel procedures, spinning techniques, solvothermal, ultra-sonic spray, and

* *Corresponding Author Email: hayder.mosa@qu.edu.iq*

pulsed laser processes, have also been used to manufacture and deposit titanium doped ZnO thin films and nanostructure [5].

In order to synthesize ZnO nanostructures using a low-cost, large-scale process, we used chemical bath deposition (CBD) for metal doping [6]. Our study group has synthesized a low-temperature CBD, focused on shape, doping concentration and aspect ratio of the nanostructures. ZnO has been reported to produce rich nanoscale features such as nanowires, nanorods and plate shaped structures [7]. This method modifies the structure to allow doping nanostructures with elements like titanium, aluminum, cadmium, and manganese, allowing for precise control of the refractive index and band gap [6].

The CBD processes. Introduction of transition metals in ZnO leads to a decrease or an increase in the band width depending on the dopant involved [8]. We present in this paper the relationship between doping concentrations and the morphology, optical proerty, ab sorption, electrical conductivity and photoluminescence charac teristics of titanium doped ZnO nanostructures synthesized by sol gel method on glass substrate with varying titanium con centration of 5- 20%. In the present work above analysis, we have made a comparative study about the doping efficiency of two groups of samples prepared from 0.1M CBD precursor solution and 1M CBD precursor solutions respectively by doping titanium with titanium chloride.

MATERIALS AND METHODS

ZnO nanostructures, both doped and undoped, were deposited on glass substrates via CBD technique. The synthesis materials were zinc nitrate hexahydrate (zinc nitrate hexahydrate, $Zn(NO_3)_2 \cdot 6H_2O$, 99.5%), zinc chloride ($ZnCl_2$, 97%), titanium chloride hexahydrate (TiCl3·6H2O, 98%), cobalt nitrate hexahydrate ($Co(NO_3)_3 \cdot 6H_2O$, 98%), and hexamethylenetetramine Prior to deposition glass substrates were thoroughly cleaned. The rinsing in dilute hydrochloric acid was followed by sequentially washing with acetone, isopropanol and deionized water. As illustrated in Fig. 1, the key steps for fabricating ZnO nanostructures via CBD method. In our lab, the CBD technique was used to successfully fabricate ZnO nanowire (NW) arrays on glass substrates. Accordingly, the substrates were immersed vertically in an equimolar solution containing either zinc nitrate hexahydrate or zinc chloride with HMTA as a capping agent at concentrations of 0.1 M or 1 M.

The reaction was allowed to proceed for six hours at 95°C in a hot oven for the best result. In the growth process, the vertically oriented nanostructures obtained were then annealed in the furnace at a temperature of 400°C for an hour. For the synthesis of titanium-doped ZnO nanostructures, titanium chloride was added to the chemical bath precursor solution at various Ti/Zn molar ratios.

The percentage of titanium incorporation in the doped samples was determined using an inductively coupled plasma mass spectrometer (ICP-MS). Table 1 as shown below, presents the data obtained with ICP-MS. Comparing the co-estimated titanium percentage in the deposited films with the titanium percentage obtained from the stoichiometric calculations it is pointed out that the titanium concentration in the ZnO samples that was doped with 1M titanium chloride is more appropriate than in the ZnO nanostructures that were doped with 0.1M titanium chloride. The limited solubility of titanium in the zinc hydroxide host lattice may explain these variations.

During the doping process, the titanium ions (Ti^{2+}) are introduced into the zinc oxide lattice. The relevant chemical equations are as follows:

$$TiCl_4(aq) \rightarrow Ti^{2+}(aq) + 4Cl^-(aq)$$

$$Zn^{2+}(aq) + Ti^{2+}(aq) + 2OH^-(aq) \rightarrow ZnTiO_3(s) + H_2O(l)$$

$$Ti^{2+}(aq) + Zn(OH)_2(s) \rightleftharpoons Zn_xTi_{1-x}O_2(s)$$

Titanium prefers tetrahedral sites during doping, and in nitrate precursors these are the (OH)4 sites while in chloride precursors the (OH) 3 Cl sites. Ti^{2+} ions are more adamant towards tetrahedral $(OH)_3Cl$ sites than $(OH)_4$ sites. The reduced Ti^{2+} incorporation is due to this selective behavior, in contrast to Zn^{2+} ions, when chloride is used to dope into TiO_2.

The incorporation of titanium into ZnO nanostructures can be explained based on the growth mechanisms associated with two different routes, which will be elaborated upon later. When using chloride salts at low molar concentrations, the growth of the nanostructures predominantly occurs along the c-axis, resulting in the formation of nanorods. In this scenario, zinc ions (Zn^{2+}) and titanium are primarily present as Zn^{2+} ions

and titanium complexes, respectively. At low concentrations, minimal electrostatic interactions between ZnO nanorod surfaces and aqueous solution complexes reduce titanium incorporation. ICP-MS analysis confirms this, showing titanium incorporation at 0.1 M concentration is substantially lower than expected [9].

When chloride salt concentrations are increased to 1 M during growth, with precursor solutions at 0.1 M and 1 M concentrations, the process produces two-dimensional (2D) nanostructures. As this growth progresses, positively charged 2D ZnO nanostructures pick up sets of negatively charged titanium hydroxide complexes ($Ti(OH)_2$), the partial charge of which is balanced by the increasingly smaller electrostatic contribution of the setting ZnO precursor. The presence of these complexes serves as capping agents to stop seed growth and allow uniform titanium incorporation into the ZnO lattice. This CBD method shows facet-selective electrostatic control that is equivalent to that observed in aluminum doped ZnO nanostructures.

RESULTS AND DISCUSSION

X-Ray Diffraction (XRD)

The crystal structure of the green-synthesized nanoparticles (NPs) or nanocomposites (NCs) was confirmed using X-ray diffraction (XRD) analysis. The distance between the crystalline levels, and the average crystallite size was determined using the Debye-Scherer. Table 2 gives the structural properties of the ZnO, TiO_2, NPs. Figs. 1, 2, and 3 show the X-ray diffraction patterns (XRD) of ZnO, TiO_2, NPs, respectively.

In ZnO nanoparticles (NPs), the three strongest diffraction peaks observed at 2-theta values of 31.811°, 34.481°, and 36.307° correspond to the Miller indices (hkl) of (100), (002), and (101), respectively. These results align with the Crystallography Open Database (COD) reference card number [96-230-0451]. The presence of these complexes serves as capping agents to stop seed growth and allow uniform titanium incorporation into the ZnO lattice. This CBD method shows facet-selective electrostatic control that is equivalent to that observed in aluminum doped ZnO nanostructures.

The TiO_2 NPs show three prominent diffraction peaks at 2-theta values of 25.16, 37.359, and 47.635, corresponding to miller indices (hkl) of (011), (004), and (020), respectively. The structure matches COD card number [96-900-8217]. The TiO_2 NPs crystallize in a tetragonal anatase phase, with crystallites averaging 22.687 nm [10].

Fig. 4 shows the prominent peak observed

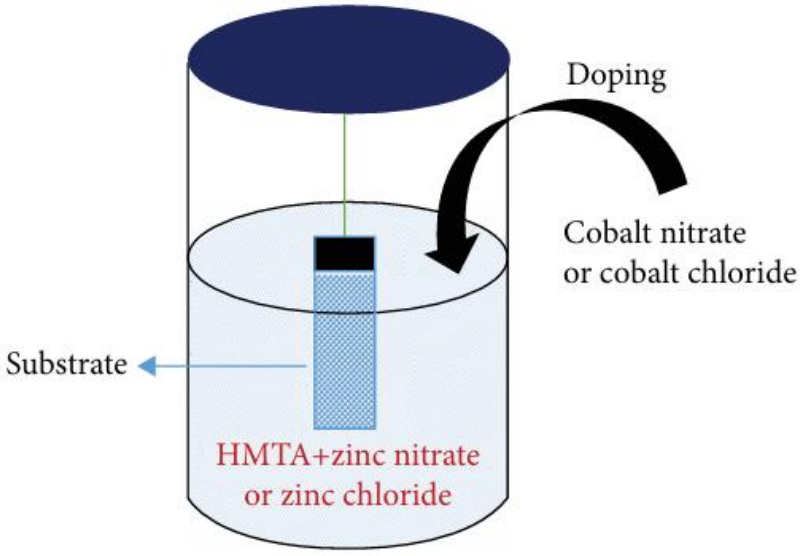

Fig. 1. CBD method for ZnO nanostructure production

around 2θ = 31.8° can be attributed to the (100) crystal plane of the hexagonal wurtzite structure of the ZnO phase. This indicates a significant fraction of zinc oxide in the mixed material. Additionally, the peak around 2θ = 25.3° corresponds to the (101) plane of the anatase polymorph of titanium dioxide (TiO_2). The presence of this peak suggests the incorporation of titanium oxide in the ZnO: TiO_2 compound.

The relative intensities of the ZnO and TiO_2 peaks provide insights into the phase composition of the mixed material. It also shows that the intensity of

Table 1. Structural properties of ZnO, TiO_2.

Sample	ZnO NPs			TiO_2 NPs		
2θ (Deg.)	Strongest three peaks			Strongest three peaks		
	31.811	34.481	36.307	25.16	37.36	47.635
hkl	100	002	101	011	004	020
FWHM (Deg.)	0.434	0.556	0.636	0.2826	0.4065	0.552
Crystallite size (nm)	19.879	15.625	13.729	30.083	21.547	16.431
Average Crystallite size (nm)	16.411			22.687		
Entry. COD	96-230-0451 (Hexagonal) "wurtzite"ZnO			96-900-8217 (tetragonal) TiO_2 "Anatase"		

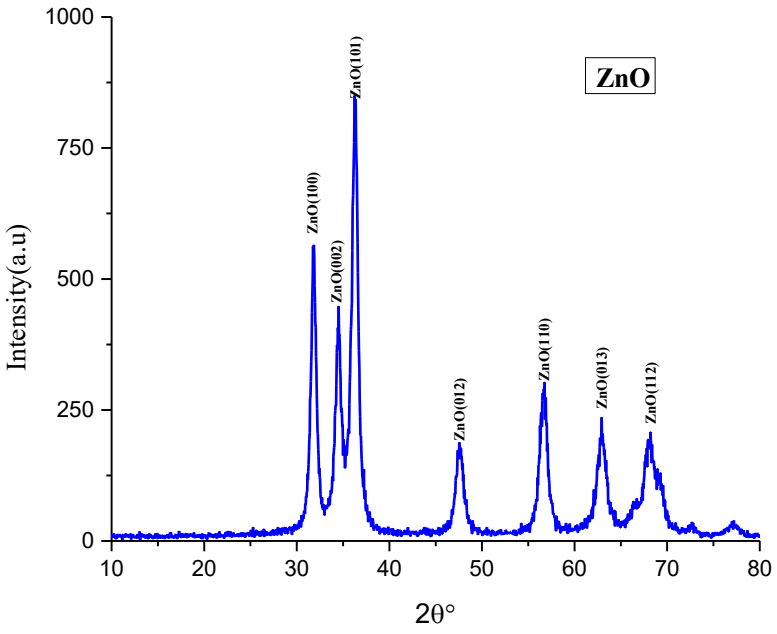

Fig. 2. XRD pattern of ZnO NPs.

the ZnO phase is much higher than the TiO_2 phase, which indicates that the ZnO represents the major phase in the sample. The broadening and asymmetry of the peaks, as well as the presence of smaller secondary peaks, indicate the possible coexistence of multiple phases, crystallite sizes, and/or defects within the ZnO: TiO_2 material. C filters Such structural features can affect the optical, electrical, and catalytic characteristics of the mixed oxide system so it could lay a good candidate for photocatalysis, optoelectronic application and gas sensor.[11].

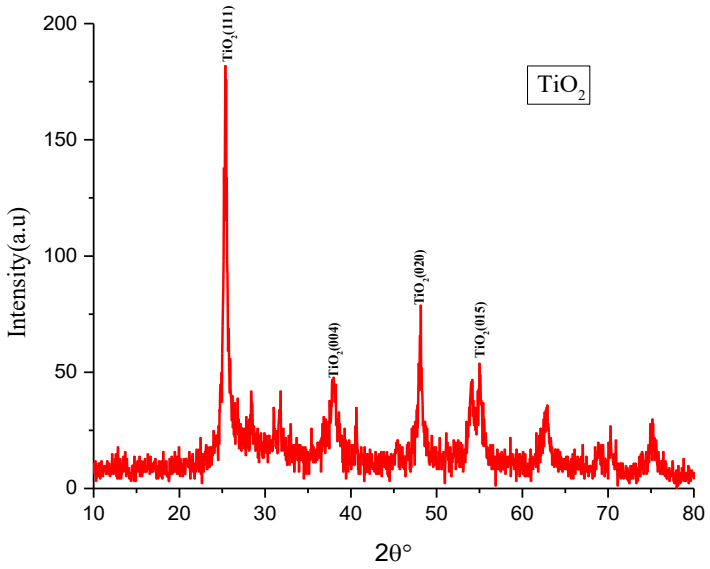

Fig. 3. XRD pattern of TiO2 NPs.

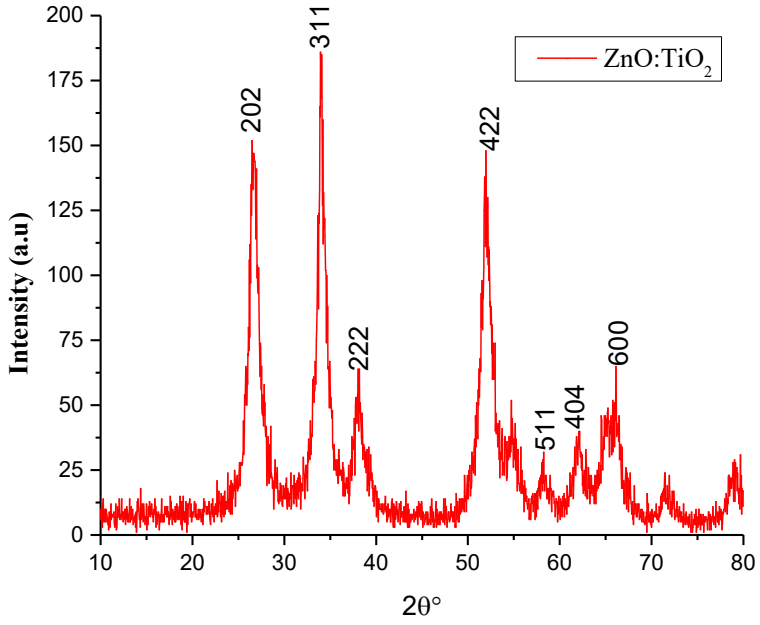

Fig. 4. XRD pattern of ZnO: TiO2 NPs.

Table 2. Structural properties of ZnO: TiO_2.

2θ (Deg.)	FWHM (Deg.)	dhkl STd.(Å)	dhkl Exp.(Å)	Crystallite Size (nm)	Average (nm)
26.66	0.80	3.35	3.34	10.21	
34.02	0.48	2.63	2.63	17.31	
38.02	0.72	2.37	2.36	11.67	
51.93	1.12	1.76	1.76	7.89	18.99
58.20	0.24	1.58	1.58	37.88	
62.1	0.72	1.50	1.49	12.88	
66.08	0.27	1.42	1.41	35.10	

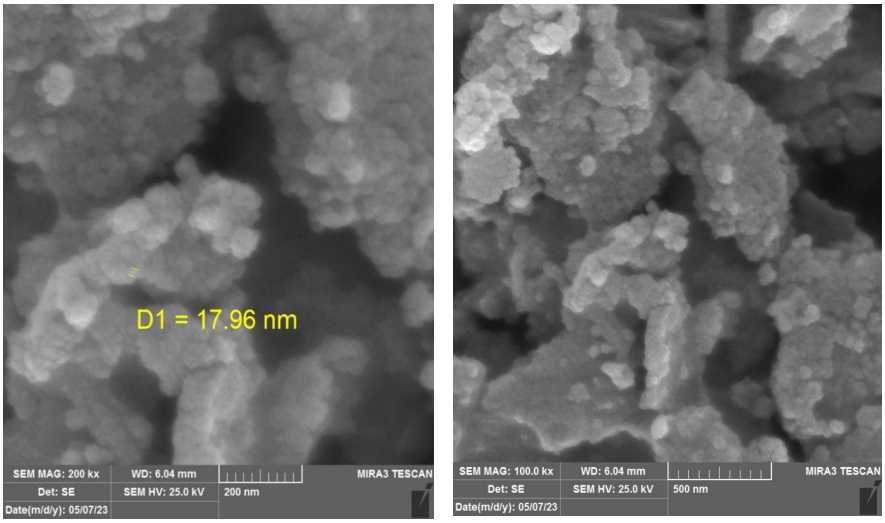

Fig. 5. FE-SEM images of the surface morphology and particle size of ZnO NPs.

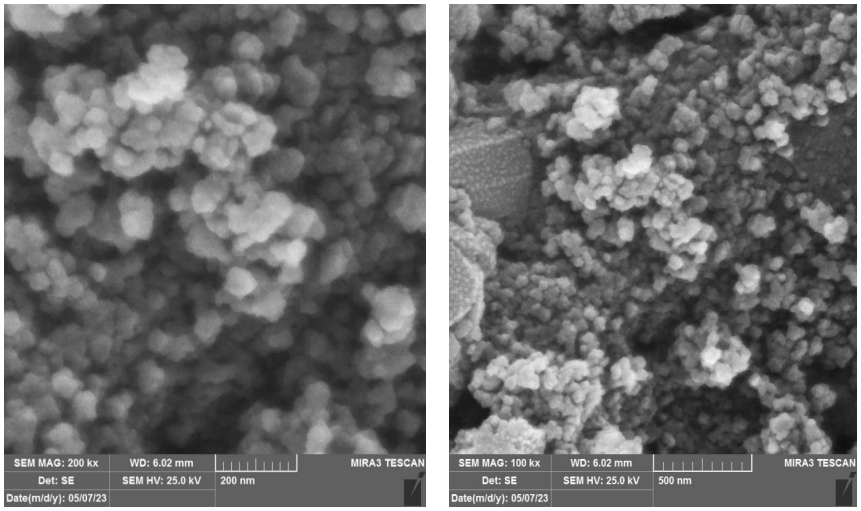

Fig. 6. FE-SEM images of the surface morphology and particle size of TiO_2 NPs.

Scanning Electron Microscopy (SEM) Analysis /EDX

The structure, size and surface features of the green synthesized nanoparticles and nanocomposites were analyzed by means of field emission scanning electron microscopy (FE-SEM) analysis. Figs. 5, 6, and 7 show the surface morphology of ZnO, TiO_2 NPs and ZnO:It is evident from the above images that the as prepared TiO_2 nanocomposite samples contained various magnifications. FESEM analysis revealed ZnO NPs with reduced aggregation of semi-spherical morphologies, averaging 17.96 nm in size. Meanwhile, FE-SEM images showed TiO_2 NPs with uniform dispersion and semi-spherical morphologies, displaying accumulations with an average particle size of ~39.1 nm.

The energy-dispersive X-ray (EDX) analysis technique, provides information about the elemental composition and chemical states present in the analyzed samples. The distinct peaks observed in the EDX spectra correspond to the characteristic binding energies of core-level electrons in the atoms composing the materials.

In the TiO_2 spectrum Fig. 8(A) , the prominent peak centered around 4.5 eV is attributed to the Ti 2p electron binding energies, indicating a significant presence of titanium in the tetravalent (Ti^{4+}) oxidation state, consistent with the titanium dioxide (TiO_2) compound. The smaller peak around 0.5 eV corresponds to the O 1s binding energies, confirming the oxygen content in the TiO_2 material. The small peak with the values of about 1 and 8 eV suggests the contamination of TiO_2 sample with a small amount of zinc.

Also in the ZnO spectrum Fig. 8B a peak detected at around 1 eV attributed to the Zn 2p electron binding energies indicate a high content of zinc in the zinc oxide (ZnO) compound. The peaks located at 0.5 eV are also reasonable with the range of O 1s binding energies of ZnO, which also indicates the presence of oxygen in ZnO material. The small peak at about 4.5 eV can be analyzed based on the results that titanium is present in a less quantity within the ZnO sample.

The ZnO: As it can be seen in the TiO_2 mixed material spectrum Fig. 8C, there is a peak at around 1eV corresponding to the Zn 2p binding energy that suggests a reasonable amount of zinc oxide in the sample. The minor peaks at 4550 cm^{-1} are the binding-energy values of Ti 2p attesting the presence of titanium oxide in the composite material. At around 0.5 eV is the oxygen 1s binding energies indicating the concentration of oxygen in both ZnO and TiO_2.

The variations in the peak intensities and positions across the three spectra reveal the differences in the elemental compositions of the TiO_2, ZnO, and ZnO: TiO_2 samples. This information is crucial for understanding the structural, optical, and electronic properties of these mixed oxide materials, which find applications in diverse fields such as photocatalysis, optoelectronics, and

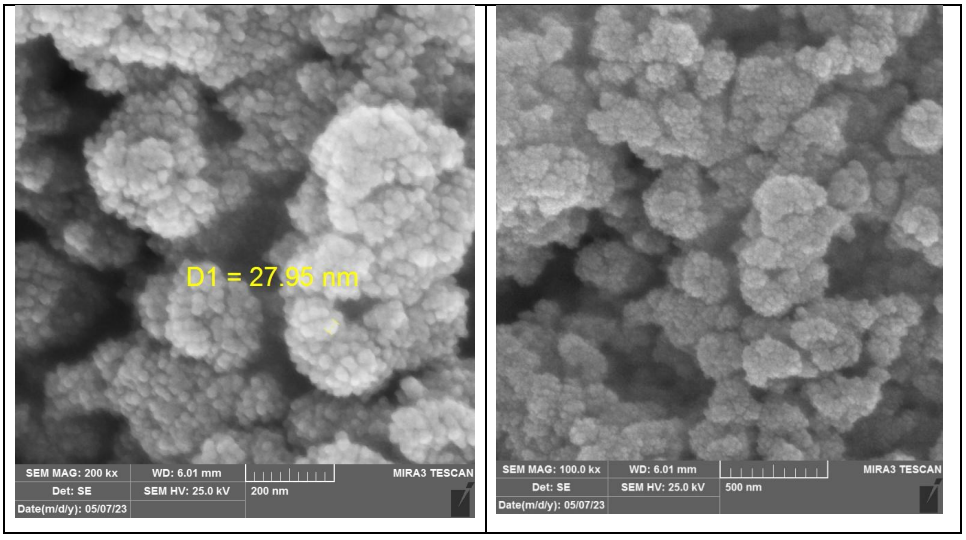

Fig. 7. FE-SEM images of the surface morphology and particle size of ZnO: TiO_2 NPs

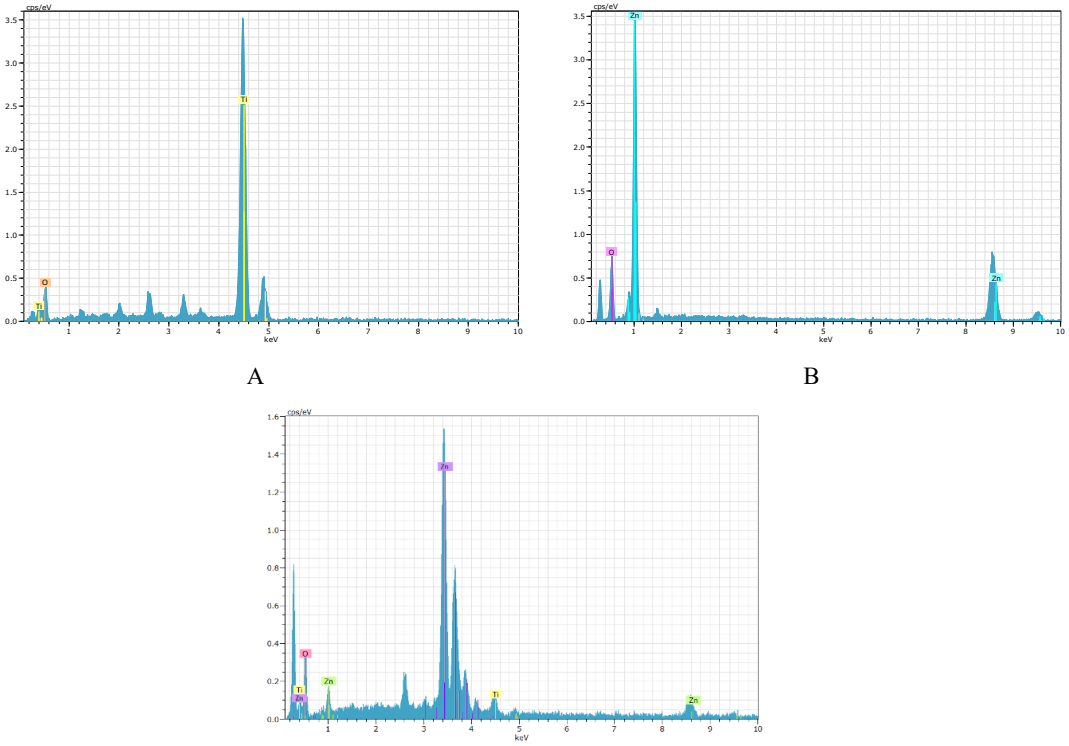

Fig. 8. EDX spectra of (A) TiO_2, (B) ZnO, and (C) ZnO-TiO_2 nanostructures showing characteristic elemental compositions.

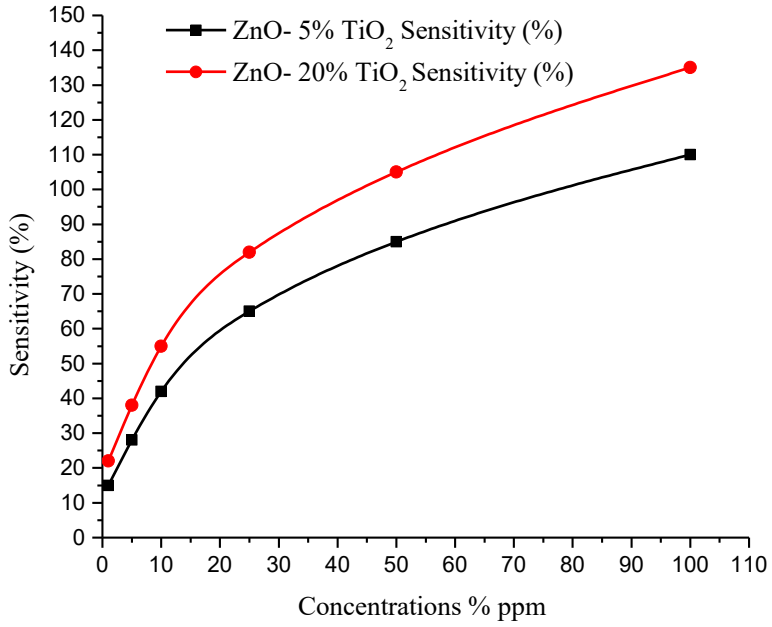

Fig. 9. NH_3 gas sensing sensitivity of ZnO-TiO_2 nanostructures at different gas concentrations.

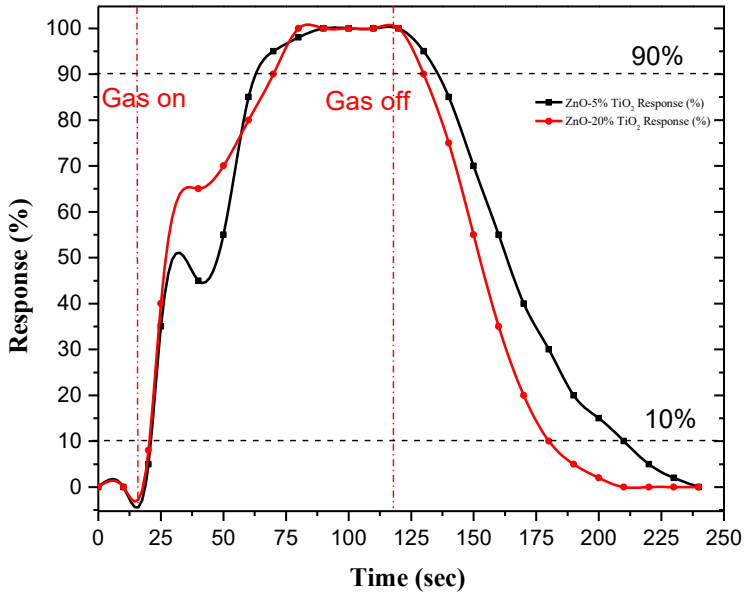

Fig. 10. Response and recovery curves of ZnO-TiO_2 (5% and 20%) sensors to NH_3 gas at room temperature, showing enhanced sensing kinetics at 20% doping.

sensor technologies.

Gass Sensor Application Results

The improved gas sensing performance of the ZnO-TiO_2 nanostructures can be explained by some factors. For sensitivity, the 20% TiO_2-doped sample performs well (135% at 100 ppm NH_3) compared to the 5% (110%) because of the bridgehead n-n heterojunctions at the ZnO-TiO_2 interface. The heterojunctions formed here result in an increased depletion of layer that changes the electron transport characteristics quite dramatically. NH_3 molecules release electrons to the sensing material when accosting the surface, which results in a wider depletion layer width and therefore a higher alteration in the resistance in the 20% sample. Higher TiO_2 content not only forms more oxygen vacancies to improve the amplification and sensitivity of gas adsorption but also generates more active sites for gas adsorption to improve sensitivity[12].

The response time, whereas the 20% TiO_2 has a shorter response time of 35s and recovery time of 95s compare with 5% sample of 45s response time and 120s recovery time only. This increase, experts say, is due to the increased density of the ZnO-TiO_2 heterojunction electron transport network. These junctions improve the electron mobility than in a homojunction thereby enabling faster charges carriers movement during the gas adsorption and desorption. Besides, the altered density of states of the surface in the 20% sample ensures proper kinetics of NH_3 molecule adsorption and desorption. The enhanced surface reactivity and the increased density of the heterojunctions directly lead to better response characteristics even better sensitivity than that presented by the detection of gas molecules enabling TiO_2 20% ZnO nanostructure to become a better gas sensing material[13].

CONCLUSION

In conclusion, low-temperature CBD synthesis of ZnO-TiO_2 nanostructures was successfully attempted, which also proved to have improved NH_3 gas sensing performance. 20% of TiO_2 inclusion enhanced the sensing performance more than that obtained with 5% dopant concentration in the ZnO matrix. The superior performance of the 20% TiO_2-doped sample was evidenced by its higher sensitivity (135% at 100 ppm NH_3) and faster response kinetics (response time: 5% sample (110% sensitivity, 45s response time, 120s recovery time) compared to 35s, 95s). This enhancement is mainly due to the formation of suitable n-n heterojunction,

high density of oxygen vacancies, and enhanced electron transport channel between the ZnO and TiO_2. Morphology analysis showed well-defined semi-spherical nanoparticles with almost uniform particle size. These results indicate that 20% TiO_2-doped ZnO nanostructure has the potential to be used for high-fast-responsend fast response NH3 gas sensors operating at room temperature.

CONFLICT OF INTEREST

The authors declare that there is no conflict of interests regarding the publication of this manuscript.

REFERENCES

1. Makableh YF, Alzubi H, Tashtoush G. Design and Optimization of the Antireflective Coating Properties of Silicon Solar Cells by Using Response Surface Methodology. Coatings. 2021;11(6):721.
2. Djurišić AB, Ng AMC, Chen XY. ZnO nanostructures for optoelectronics: Material properties and device applications. Progress in Quantum Electronics. 2010;34(4):191-259.
3. Akgül FA. Influence of Ti doping on ZnO nanocomposites: Synthesis and structural characterization. Composites Part B: Engineering. 2016;91:589-594.
4. Bui VKH, Park D, Lee Y-C. Chitosan Combined with ZnO, TiO_2 and Ag Nanoparticles for Antimicrobial Wound Healing Applications: A Mini Review of the Research Trends. Polymers. 2017;9(1):21.
5. Vidor FF, Wirth GI, Hilleringmann U. Low temperature fabrication of a ZnO nanoparticle thin-film transistor suitable for flexible electronics. Microelectronics Reliability. 2014;54(12):2760-2765.
6. Di Mari GM, La Matta V, Strano V, Reitano R, Cerruti P, Filippone G, et al. Optimized Chemical Bath Deposition for Low Cost, Scalable, and Environmentally Sustainable Synthesis of Star-Like ZnO Nanostructures. ACS omega. 2024;9(37):38591-38598.
7. Djurišić AB, Chen X, Leung YH, Man Ching Ng A. ZnO nanostructures: growth, properties and applications. Journal of Materials Chemistry. 2012;22(14):6526.
8. Kaphle A, Reed T, Apblett A, Hari P. Doping Efficiency in Cobalt-Doped ZnO Nanostructured Materials. Journal of Nanomaterials. 2019;2019:1-13.
9. Baruah S, Dutta J. Hydrothermal growth of ZnO nanostructures. Science and technology of advanced materials. 2009;10(1):013001-013001.
10. El-Desoky MM, Morad I, Wasfy MH, Mansour AF. Synthesis, structural and electrical properties of PVA/TiO_2 nanocomposite films with different TiO_2 phases prepared by sol–gel technique. Journal of Materials Science: Materials in Electronics. 2020;31(20):17574-17584.
11. Araújo ES, Libardi J, Faia PM, de Oliveira HP. Hybrid ZnO/TiO_2 Loaded in Electrospun Polymeric Fibers as Photocatalyst. Journal of Chemistry. 2015;2015:1-10.
12. Oleiwi DHF, Abdul Kareem I. Enhancing Gas Sensing Performance of TiO_2-ZnO nanostructures: Effect of ZnO Concentration. Ibn AL-Haitham Journal For Pure and Applied Sciences. 2023;36(4):137-146.
13. Liu H, Shen W, Chen X, Corriou J-P. A high-performance NH3 gas sensor based on TiO_2 quantum dot clusters with ppb level detection limit at room temperature. Journal of Materials Science: Materials in Electronics. 2018;29(21):18380-18387.